Journal of Materials Chemistry B

PAPER

View Article Online
View Journal | View Issue

Cite this: J. Mater. Chem. B, 2014, 2, 4280

Peptide microarrays for the discovery of bioactive surfaces that guide cellular processes: a single step azide–alkyne "click" chemistry approach†

Douglas Zhang and Kristopher A. Kilian*

Cell behavior *in vivo* is guided by a complex microenvironment containing many different molecules including extracellular matrix (ECM) proteins, growth factors, and proteoglycans. Controlling the interaction between these various components at the cell–material interface will be invaluable in developing new materials for biomedical devices and tissue engineering applications. We report a single step approach to forming mixed peptide conjugated self-assembled monolayers on gold using copper-catalyzed azide–alkyne cycloaddition chemistry to study the combinatorial effects of different peptide ligands on cellular processes. We synthesized ECM adhesion peptides (YIGSR, GRGDS), a bone morphogenetic protein 7 (BMP-7) derived peptide (KPSSAPTQLN), and a heparin binding peptide (KRSR), and arrayed them, alone and in combination, onto gold coated coverslips. SAMs were characterized by X-ray photoelectron spectroscopy (XPS) and matrix-assisted laser desorption/ionization (MALDI) mass spectrometry, and arrayed peptide combinations were seen to differentially bind to adipose derived stem cells (ADSCs) and mouse embryonic fibroblasts (MEFs). We further investigated the osteogenesis of ADSCs on SAMs containing combinations of adhesion peptide and BMP-7 peptide in both standard culture and osteogenic differentiation media. We demonstrate enhanced expression of osteogenic markers Runx2 and osteopontin when ADSCs are adherent to BMP-7 derived peptide alone or in combination with ECM adhesion peptides. The platform presented here enables immobilization of multiple peptides in a single step using a commercially available microarray spotter which will prove useful in fabricating biomolecule interfaces for cell biology studies and biochemical assays.

Received 7th March 2014
Accepted 19th May 2014

DOI: 10.1039/c4tb00375f

www.rsc.org/MaterialsB

Introduction

Autologous stem cells – multipotent cells derived from a patient's own body – offer broad therapeutic potential due to their immunocompatibility, ability to differentiate into multiple cell types, and lack of ethical issues related to their derivatization. Bone marrow derived stem cells (BMSCs), first observed by Friedenstein and co-workers,[1] are a well characterized cell type known to differentiate into multiple cell types important to tissue engineering, including cartilage, bone, tendon, and muscle.[2–4] Recently, these mesenchymal stem cells have been isolated in nearly all tissues and organs in the body.[5] Multipotent stem cells within adipose tissue, adipose-derived stem cells (ADSCs) have recently gained popularity as adipose tissue is widely available and easily obtainable.[6–8] While these cells hold much promise, precise control and understanding of the complex signaling between the cell and the extracellular matrix (ECM) will be important for clinical translation. When biomaterials are exposed to biological environments *in vivo* or growth media *in vitro*, ECM matrix proteins can nonspecifically adsorb to the surface, allowing cells to interact with the biomaterial surface through the adsorbed ECM proteins.[9] ECM proteins such as fibronectin, vitronectin, and laminin are often used for surface modifications, and combinations of these and other proteins are an attractive strategy for recapitulating the complex composition of the *in vivo* microenvironment. For instance, Langer and colleagues used combinations of leukemia-inhibitory factor, fibronectin, laminin, and fibroblast growth factor 4 substrates to investigate murine embryonic stem cell self-renewal and differentiation.[10] Bhatia and colleagues spotted 32 combinations of five ECM molecules (collagen I, collagen III, collagen IV, laminin, and fibronectin) onto acrylamide hydrogels and assessed the differentiation of mature, primary rat hepatocytes, and mouse ES cells.[11] Both studies showed that ECM molecules can have synergistic as well as antagonistic effects on self-renewal and differentiation, demonstrating the importance of cross-talk between integrin, growth factor, and matrix molecules.

Department of Materials Science and Engineering, University of Illinois, Urbana-Champaign, Illinois 61801, USA. E-mail: kakilian@illinois.edu

† Electronic supplementary information (ESI) available: Additional information about HPLC purification; AFM measurements of monolayers; 10 day image demonstrating long term culture capabilities of spotted areas; example of how surface coverage is quantified; and ellipsometry measurements is provided. See DOI: 10.1039/c4tb00375f

The discovery that the arginine-glycine-aspartic acid (RGD) amino acid sequence on the binding domain of fibronectin could form an essential recognition site for cells[12] spurred research into discovering other minimum binding sequences that had similar selectivity for cell integrins. Although less effective than whole proteins alone, peptides offer the advantage of being short, easily synthesized, and integrin-specific.[13] Peptides are cost-efficient, easy to synthesize and purify, and able to be conjugated in a spatially defined manner.[14] In addition, very low concentrations of peptides are needed for maximal spreading ($\sim$1 fmol cm^{-2}).[15] Materials to model ECM must incorporate several design elements. They should be well defined, allow for ECM protein or peptide immobilization, and present an inert background to nonspecific adsorption. One of the best and most studied systems are self-assembled monolayers (SAMs) of alkanethiolates on gold.[16] SAMs form well-ordered close-packed structures in the presence of gold, and ECM protein mimics can be introduced by a simple mixture of terminally substituted alkanethiols.[14,17] Hudalla and Murphy for instance, used a mixture of carboxyl and azide terminated alkanethiolates to immobilize adhesion peptide RGDSP as well as TYRSRKY in order to explore the synergistic effects of these peptides on cell adhesion.[18]

Ligand presentation clearly plays a role in stem cell fate decision and function, and testing single candidate peptides and proteins is instructive, but in order to discover novel ligands, high-throughput approaches to model ECM are required.[19] Early work by Langer and colleagues exploited the use of robotic fluid handling to create arrays of polyacrylate monomers to study the effect of polymer–cell interactions.[10] Lutolf and co-workers used a DNA spotter to create cell niche microarray spots with modular stiffness (1–50 kPa) per well, along with various combinations of proteins. They found that certain combinations of ECM adhesion protein, growth factor, and stiffness could influence proliferation, quiescence, and death of neural stem cells.[20] Kiessling and colleagues applied SAMs on gold into an array type format investigating the effects of various peptide ligands on stem cell culture.[21] Using phage display based on the "biopanning and rapid analysis of selective interactive ligands" (BRASIL) technique,[22] they were able to identify six novel peptides that possessed embryonal carcinoma cell binding capabilities.[23] Recently, Yousaf and colleagues microarrayed a variety of small molecules and peptides and investigated ligand density effects on the differentiation of MSCs.[24]

In this paper we present a microarray strategy using self-assembled monolayers of alkanethiolates on gold to form well-defined regions of various combinations of peptides in a single step. The peptides are conjugated to the SAM *via* copper I catalyzed azide–alkyne "click" cycloaddition (CuAAC). We investigated a cell adhesion peptide (YIGSR), a bone morphogenetic protein (BMP) growth factor derived peptide (KPSSAPTQLN), and a heparin binding peptide (KRSR). By varying the ratio of peptides before spotting, we can investigate combinatorial effects of these peptides on the adhesion characteristics on two different cell types, mouse embryonic fibroblasts (MEFs) and adipose derived stem cells (ADSCs). This biofunctionalization strategy can be applied to any peptide or small molecule containing a pendant alkyne group. We further investigate the differentiation of ADSCs on a combination of peptides and show that surfaces presenting the BMP-7 derived peptide alone or in combination with other adhesion peptides can enhance osteogenic markers after 3 weeks in standard culture media.

Experimental section

Materials

Cover glass substrates were purchased from Fisher Scientific. All chemicals, unless noted otherwise, were purchased from Sigma Aldrich, of analytical grade and used as received. 11-(2-{2-[2-(2-Azido-ethoxy)-ethoxy]-ethoxy}-ethoxy)-undecane-1-thiol (referred to herein as HS-C11-EG4-N3) was purchased from Prochimia (Sopot, Poland, TH 008-m11.n4-0.2). Triethylene glycol mono-11-mercaptoundecyl ether (referred to herein as HS-C11-EG3) was purchased from Sigma Aldrich (673110). Tissue culture plastic ware was purchased from USA Scientific. Peptide synthesis reagents and amino acids were purchased from Anaspec. Cell culture media and reagents were purchased from Gibco. Sulfo-NHS-LC-biotin (Pierce) and streptavidin-Cy3 (Life Technologies) were a kind gift from Dr Paul R. Selvin in the Department of Physics at the University of Illinois at Urbana-Champaign. Human adipose-derived stem cells (ADSCs) (PT-5006) and differentiation media were purchased from Lonza. Mouse embryonic fibroblasts (MEFs) (C57BL/6 4M untreated) were purchased from globalstem. ADSCs were isolated from lipoaspirates collected during surgical liposuction procedures. ADSCs were tested for purity by Lonza, and were positive for CD13, CD29, CD44, CD73, CD90, CD105, CD166 by flow cytometry, and had the ability to differentiate into osteogenic, chondrogenic, adipogenic lineages (http://www.lonza.com). The use of human ADSCs in this work was reviewed and approved by the University of Illinois at Urbana-Champaign Biological Safety Institutional Review Board.

Peptide synthesis

Peptides were synthesized manually by standard Fmoc solid-phase methodology. N-terminal fluorenylmethyloxycarbonyl (Fmoc) protected rink amide resin was deprotected with 20% piperidine in *N*′,*N*′-dimethylformamide (DMF) for 15 min. The solvent was filtered with a vacuum manifold, and resin was washed 4 times with DMF. A solution containing 3 equivalents of the amino acid, benzotriazol-1-yl-oxytripyrrolidinophosphonium hexafluorophosphate (PyBOP), and *N*-methylmorpholine in DMF was added to each tube for a 1 h incubation at room temperature. The solutions were then filtered, washed 4 times with DMF, and the next Fmoc was deprotected. After all amino acid residues were coupled, the peptides were capped with a propargyl-PEG-NHS ester (Quanta Biodesign, 10511) in DMF overnight. The resin was then washed 4 times with DMF and 4 times with ethanol before cleaving with a cocktail containing 95% trifluoroacetic acid (TFA), 2.5% H_2O, and 2.5% triisopropylsilane (TIS) and incubating at room temperature for 3 h. The

resulting solution was evaporated by flowing air over the tube for 30 minutes. The resultant precipitate was re-dissolved in 1 mL TFA, and re-precipitated in 9 mL ice-cold diethyl ether. After 3 additional dissolve-precipitate steps, the residues were dissolved in water and lyophilized overnight. Bioactive peptides Tyr-Ile-Gly-Ser-Arg (YIGSR), Lys-Pro-Ser-Ser-Ala-Pro-Thr-Gln-Leu-Asn (KPSSAPTQLN, herein referred to as KPSS), Lys-Arg-Ser-Arg (KRSR), Gly-Arg-Gly-Asp-Ser (GRGDS) and scrambled control peptide Gly-Arg-Asp-Gly-Ser (GRDGS) were synthesized. Final products were analyzed with low resolution electrospray ionization (ESI) (Waters Quattro II) and semipreparative reversed-phase high-performance liquid chromatography (RP-HPLC) (Perkin-Elmer Flexar). All peptides used were purified to >90% purity as assessed by HPLC.

Surface preparation

Glass coverslips were cleaned by sonicating 20 min in ethanol and dried under air. 5 nm of Ti followed by 20 nm of Au were then deposited on the surface by electron beam deposition. Gold surfaces were stored in a dessicator for up to two weeks before use. Prior to microarray spotting, gold surfaces were cut to fit into 6-well plates, cleaned by briefly sonicating for 1 min in glacial acetic acid and 1 min in ethanol, and mounted onto 75 × 25 mm microscope slides by applying a thin layer of ethanol to the interface.

Microarray printing

Stock solutions of peptide ligand (1 mM in H_2O), Tris[(1-benzyl-1*H*-1,2,3-triazol-4-yl)methyl]amine (TBTA) (10 mM in DMSO–*t*-butyl alcohol (3 : 1)), and azide-terminated alkanethiolate solution (HS-C11-EG4-N3/HS-C11-EG3, 15% azide mole fraction in ethanol) were prepared and stored at −20 °C. Copper solution (10 mM CuBr, 10 mM sodium ascorbate in DMSO) was prepared fresh prior to click modification. Click solution was prepared by combining stock TBTA solution with fresh CuBr solution (2 : 1 v/v). Reaction vials containing peptide ligand (5 μL), click solution (5 μL), and azide-terminated alkanethiolate solution (10 μL) were prepared and incubated at 37 °C for 1 h. These solutions were transferred to a 384-well plate and printed in subarray format on the gold-coated surfaces using a Gene Machines OGR-03 OmniGrid Microarrayer. The substrate is removed from the microscope slide and thoroughly rinsed with DI H_2O followed by ethanol. After 4 rinse steps, printed substrates were immersed in a 0.1% ethylenediaminetetraacetic acid (EDTA) solution for 20 minutes, followed by another 4 rinse steps. Substrates were then immersed in a HS-C11-EG3 solution to render the non-printed regions inert to nonspecific adsorption.

Long-term SAMs

For assessing differentiation of ADSCs over 21 days, we cultured cells on selected peptide combinations. Au surfaces were immersed in 15% HS-C11-EG4-N3/HS-C11-EG3 overnight to form monolayers. Surfaces are rinsed with ethanol and cut to fit into 24-well culture plates. Peptides are conjugated to the monolayers by incubation of click solution and peptide ligand (1 : 1, 10 μL) at room temperature for 12 h.

Cell culture

Human ADSCs were cultured in Dulbecco's Modified Eagle's Medium (DMEM) low glucose (1 g mL^{-1}) media supplemented with 10% fetal bovine serum (Invitrogen), 1% penicillin/streptomycin (p/s), media changed every 3–4 days and passaged at ~80% confluency using 0.25% trypsin : EDTA (Gibco). MEFs were cultured in Dulbecco's Modified Eagle's Medium (DMEM) high glucose (4.5 g mL^{-1}) media supplemented with 10% fetal bovine serum (Invitrogen), 1% penicillin/streptomycin (p/s) and passaged at ~80% confluency using 0.05% trypsin : EDTA (Gibco). Passage 4–6 ADSCs and passage 6 MEFs were seeded onto microarrayed and non-microarrayed surfaces at a cell density ~15 000 cells per cm^2 for ADSCs and ~30 000 cells per cm^2 for MEFs. After 1 h incubation at 37 °C and 5% CO_2, non-adherent cells were aspirated, surfaces were washed, and fresh media added.

Cell differentiation

For long-term differentiation studies, human ADSCs were seeded on non-microarrayed SAM surfaces (~10 000 cells per cm^2) and cultured in basal media (low glucose DMEM supplemented with 1% p/s and 10% FBS) or osteogenic media (low glucose DMEM containing FBS, gentamicin/amphotericin, L-glutamine, dexamethasone, ascorbate and β-glycerophosphate). Media was changed every 3–4 days for 21 days.

Cell attachment quantification

Quantification of ADSC and MEF spot coverage in brightfield images was performed using ImageJ (NIH). The "Image Edge" plugin developed by Thomas Boudier (available at http://www.snv.jussieu.fr/~wboudier/softs.html) was applied to images of array spots and then a threshold was applied to select areas marked by cells. Circular regions of interest (ROIs) were sized to the same dimensions of an array spot and were used to define areas for measurement (Fig. S3†). A minimum of 3 subarrays, each containing at least 4 spots per peptide combination, were measured.

Immunohistochemistry and fluorescence assays

Cells were fixed with 4% paraformaldehyde for 20 min, permeabilized with 0.1% Triton X-100 in PBS for 30 min, and blocked with 1% BSA in PBS for 15 min. Primary antibody labeling was performed in 1% BSA in PBS solution overnight at 4 °C with rabbit anti-osteopontin (Abcam, 1 : 500 dilution) and mouse anti-Runx2 (Abcam, 1 : 500 dilution). Secondary antibody labeling was performed similarly in 5% goat serum containing 1% BSA in PBS solution with tetramethylrhodamine-conjugated anti-rabbit IgG antibody and Alexa Fluor 647-conjugated anti-mouse IgG antibody (1 : 500 dilution) along with Alexa Fluor 488-phalloidin (1 : 250 dilution) and DAPI (1 : 5000 dilution) for 20 min at 37 °C. Peptide self-assembled monolayers with terminal lysine residues were exposed to a

1 mM solution of sulfo-NHS-LC-biotin in 1 × PBS for 30 minutes followed by rinsing. The functionalized surfaces were incubated with Cy3-Streptavidin for 30 minutes followed by copious rinsing in 1 × PBS prior to microscopy.

Microscopy

Brightfield images were taken with a MOTIC AE31 inverted microscope with a Moticam 3 Digital Color Camera. Immunofluorescent imaging was performed on an IN Cell Analyzer 2000 (GE). A minimum of 16 fields of view were taken for each sample condition. Immunofluorescent images were analyzed using ImageJ. Regions of interest for Runx2 and osteopontin were selected by outlining nuclei in the DAPI channel. Mean integrated density of every cell localized to the region of interest was averaged for each replicate. To normalize fluorescence intensity for cells of differing sizes, we chose to only report the average fluorescent intensity localized at the nucleus. At least three independent experiments each with triplicate samples were performed to verify results. One-way ANOVA was performed using OriginPro software.

Infrared spectra (IR)

IR spectra was collected on a Perkin Elmer 100 serial FTIR spectrophotometer calibrated with polystyrene film.

Mass spectrometry

Mass analysis was performed using a Bruker UltrafleXtreme time-of-flight (TOF) mass spectrometer (Bruker) in positive reflector mode. 1 μL of each spotting solution was manually pipetted onto a small Au substrate and allowed to sit 30 min. SAM surfaces were rinsed and attached to a custom MALDI plate using a small spot of high vacuum grease (Dow Corning). 1 μL of α-cyano-4-hydroxycinnamic acid (HCCA, Bruker) matrix dissolved in mixture of 1 : 2 acetonitrile (ACN) : 0.1% trifluoroacetic acid (TFA) in ultra pure water was spotted to the surface of each SAM. Mass spectra were obtained at 100 μm resolution with each spot summed from 200 laser shots. Mass calibration was done with peptide calibration standard II (Bruker). Spectra was analyzed with flexAnalysis software (Bruker) and replotted with Origin (OriginLab).

X-ray photoelectron spectroscopy (XPS)

XPS data were acquired using a Kratos Axis ULTRA Imaging X-ray Photoelectron Spectrometer (Kratos Analytical Ltd.) with a monochromatic Al Kα source (1486.6 eV). Spectra was obtained in spectroscopy mode with a base pressure below 1×10^{-8} Torr. The take-off angle was set to 90°, and an analyzer slot aperture of 0.3 mm × 0.7 mm. Survey spectra were collected from 0 to 1100 eV with a 1.0 eV step size, 100 ms dwell time and an analyzer pass energy of 160 eV. High-resolution spectra were obtained for photoelectrons emitted from C 1s, N 1s, and Au 4f with a 0.1 eV step size, a dwell time of 100 ms, and analyzer pass energy of 40 eV. Electron binding energies were calibrated with respect to the Au 4f peak at 84.0 eV. All XPS analysis was performed with CasaXPS software. Analysis of spectra involved background subtraction using a Shirley routine and a subsequent fitting of Gaussian–Lorentzian line-curves using a Marquardt–Levenberg optimization algorithm.

Ellipsometry

Ellipsometric measurements were made with a J. A. Woollam VASE spectroscopic ellipsometer with wavelength of 500–800 nm and incident angles of 65, 70, and 75°. Thicknesses were computed with a planar two-layer (substrate, monolayer) Cauchy model with refractive index set at 1.40 for the monolayer.[25]

Atomic force microscopy (AFM)

The measurements were carried out with an Asylum Research MFP-3D AFM in non-contact (tapping) mode. AFM scans were performed in air. A rotated, monolithic silicon tip (BudgetSensors) was used.

Results and discussion

Development of peptide derivatized self-assembled monolayers on gold surfaces

Peptides were synthesized manually using standard Fmoc solid-phase methodology and purified *via* HPLC (Fig. S1†). We chose to cap our peptides with an alkyne-containing capping reagent to yield a terminal alkyne that is amenable to bioconjugation to an azide terminated surface. This strategy allows us to investigate combinations of peptides by simply mixing stock peptide solutions in the desired ratios.[26]

Within each well of a 384-well plate, we mixed together a stock solution of HS-C11-EG4-N3, HS-C11-EG3, a peptide or combination of peptides capped with an alkyne reagent, and a buffer containing Cu(I), TBTA, and sodium ascorbate to catalyze the cycloaddition reaction. The plate was incubated for one hour at 37 °C before printing. Using an OmniGrid Microarrayer, the microarray tips act as features, depositing small nanoliter scale volumes onto the surface of the gold. Alkanethiols in the spotted solutions adsorb immediately to the gold to form self-assembled monolayers within the printed circular regions (Fig. 1). The substrate was subsequently washed and immersed in a background solution of HS-C11-EG3 to render the non-spotted regions inert to protein adsorption.

FTIR was used to monitor the completion of the peptide conjugation to the HS-C11-EG4-N3 in solution (Fig. 2) prior to spotting. After 1 h at 37 °C we observed that the azide peak at λ 2110 cm^{-1} completely disappears, demonstrating fast conjugation of the alkyne-terminated peptide with the azide-terminated alkanethiolate. After spotting the mixture on the gold substrate, XPS was used to confirm the presence of a monolayer as well as conjugation of peptides. The underivatized monolayer surface containing 15% HS-C11-EG4-N3 to HS-C11-EG3 shows low atomic % of nitrogen species (Fig. 3a and Table 1) as expected for the diluted azide monomer. The C 1s narrow scan of this surface reveals the presence of C–C to C–O peaks in percentages of 65.2% to 34.8% respectively (Fig. 3b), in close agreement with an expected percentages of 65%

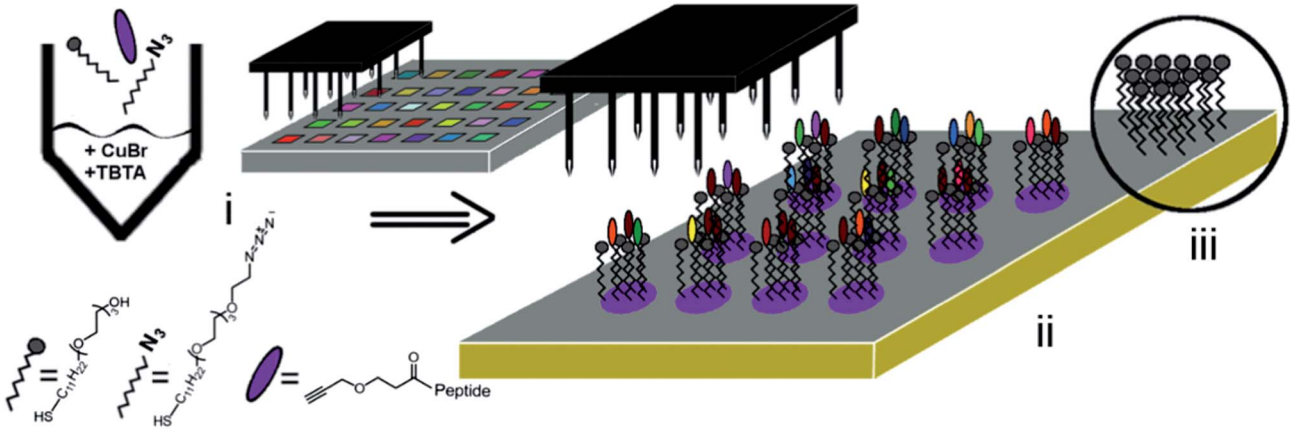

Fig. 1 Scheme for spotting of microarray surfaces. A 384-well plate containing mixed ratios of ECM, proteoglycan, and morphogen peptides (i) defines the spot features on gold substrates (ii). After spotting, the surfaces are washed and backfilled with a non-fouling background layer (iii).

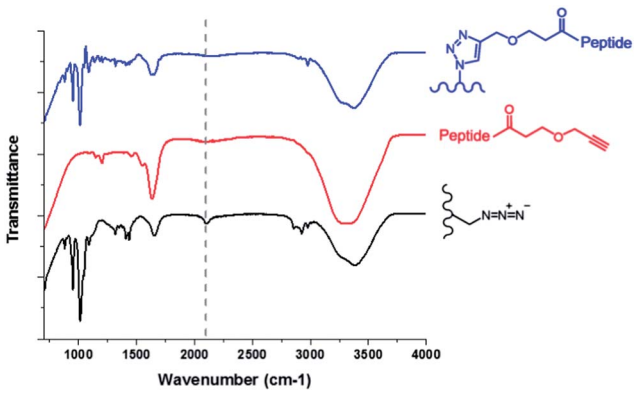

Fig. 2 Conjugation of alkyne-terminated peptide KPSSAPTQLN to azide-terminated SAM assessed in solution *via* FTIR. A control solution of HS-C11-EG4-N3 dissolved in H_2O : ethanol : DMSO at concentration 40 mM (solid black line) shows clear azide peak at 2110 cm^{-1}. Control peptide in H_2O at concentration 40 mM (solid red line) and conjugate after 1 hour (solid blue line) demonstrate disappearance of azide groups (ν = 2110 cm^{-1}). Reactions were performed under the same microarray printing experimental conditions.

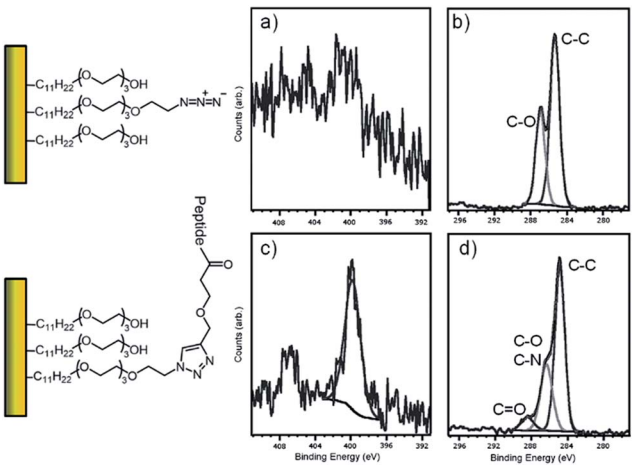

Fig. 3 XPS data for azide-terminating surfaces and peptide-conjugated surfaces: N 1s narrow scan of surfaces before (a) and after (c) peptide conjugation; C 1s narrow scan of surfaces before (b) and after (d) peptide conjugation.

to 35%. After cycloaddition reaction, surfaces included noticeable increases in the N 1s narrow scan spectra (Fig. 3c), as well as the appearance of a C=O peak in the C 1s spectra (Fig. 3d).

Mass spectrometry of self-assembled monolayers on gold, a technique termed self-assembled monolayer desorption ionization (SAMDI) by Mrksich and co-workers,[27] is an effective method for characterizing the products from interfacial reactions on SAMs.[28] To demonstrate that spotting the reaction solution directly onto a gold slide will enable robust monolayer formation, we simulated printing conditions by transferring 1 μL of spotting solution onto the surface of a cleaned gold surface. After 30 minutes, this surface was cleaned and mounted on a custom plate for matrix assisted laser desorption ionization (MALDI) mass spectrometry. MALDI analysis reveals peaks corresponding to the conjugated peptide-alkanethiolate species, as well as several disulfide peaks formed either between two conjugated peptide-alkanethiolate species, or with the HS-C11-EG3 diluent. For instance, spotted KPSSAPTQLN shows a single peptide-alkanethiolate conjugate at m/z 1562.2 as well as the disulfide at 3114.2, and another disulfide corresponding to the addition of the EG3-terminated background alkanethiolate at 1893.6 (Fig. 4a).

Table 1 XPS quantification of peak areas for surfaces before and after conjugation

Surface	Binding energy (eV)		Surface concentration (%)
Azide SAM	C 1s	285.3	65.2 (C–C)
	C 1s	286.9	34.8 (C–O)
Peptide SAM	C 1s	284.8	63.0 (C–C)
	C 1s	286.3	30.5 (C–O/C–N)
	C 1s	288.4	6.5 (C=O)
	N 1s	400.0	

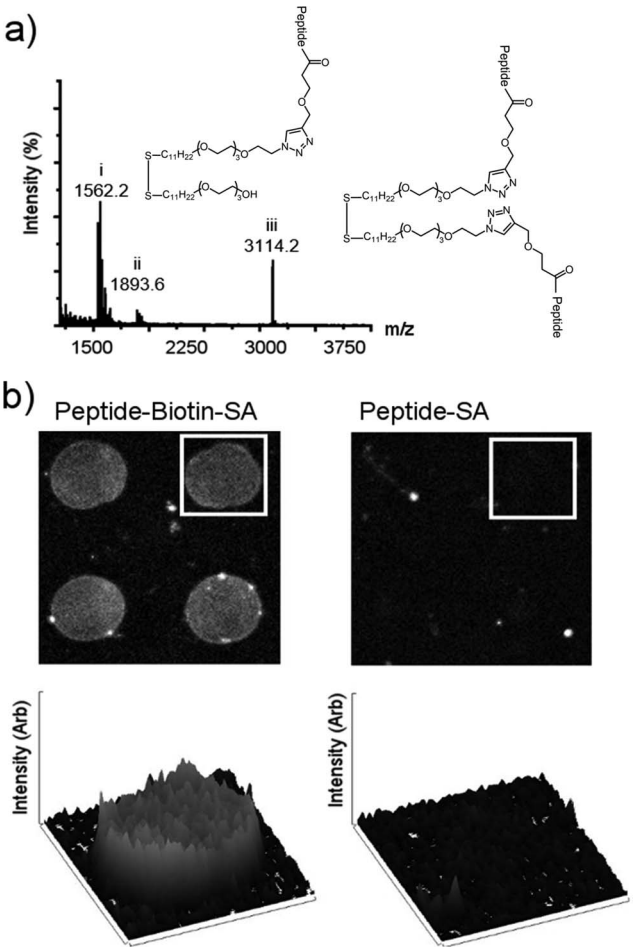

Fig. 4 Characteristic SAMDI spectra for peptide KPSSAPTQLN. We generally observed up to three peaks for each peptide conjugated SAM (a). Species (i) corresponds to the conjugated peptide species, while species (ii) and (iii) represent the disulfides formed with either the HS-C11-EG3 background, or two peptide conjugated alkanethiolates respectively. Spotted regions of a peptide (FHRRIKA) containing a lysine adjacent to the distal end of the SAM (b) is biotinylated with a biotin-NHS reagent. After incubation in the presence of streptavidin-Cy3 (SA) for 30 min at room temperature, we see uniform fluorescence across the peptide spots. Non-biotinylated spotted regions incubated with SA show no fluorescence.

To further verify that we are forming SAMs using the microarraying strategy, we performed ellipsometry and atomic force microscopy on microarray spots. The ellipsometric thickness of a SAM containing just HS-C11-EG3 was measured to be approximately 1.22 nm. This thickness increased to 1.49 nm for the monolayer surface containing 15% HS-C11-EG4-N3 to HS-C11-EG3, and 1.66 nm when a peptide (KPSSAPTQLN) was conjugated (Table S1†). The thickness was calculated assuming a parallel, homogeneous, two-layer (monolayer, substrate) model with an assumed refractive index of 1.4 for the organic layer.[25] Our observed thicknesses are comparable to those of previously reported SAMs of similar structure.[25,29] AFM measurements at the edge of one of the SAM spots show a height difference of approximately 1.5 nm between the formed SAM and the gold substrate, in good agreement with our ellipsometry measurements (Fig. S2†).

To assess whether the peptides are homogenously distributed when SAMs are formed, we spotted arrays of a peptide containing a lysine residue in proximity to the distal end (FHRRIKA). We biotinylated the free amine of the lysine with a sulfo-NHS-biotin reagent followed by incubation in the presence of a Cy3-conjugated streptavidin. A control array of the peptide was incubated with the Cy3-streptavidin without prior biotinylation (Fig. 4b). We see uniform fluorescence across our SAM spots demonstrating that the peptide is evenly distributed. However, we cannot rule out the possibility that the peptide-conjugated alkanethiols may phase separate into domains, as has been reported for two component SAMs.[30,31] No fluorescence is seen on peptide spots without prior biotinylation, highlighting the ability of the SAMs at resisting non-specific protein adsorption.[32]

Previous work by Chelmowski *et al.* demonstrated that click chemistry is well suited for the production of peptide-based SAMs due to its high selectivity and tolerance for all functional side groups in peptides.[32] Furthermore, they showed that performing the click reaction in solution is more efficient than conjugation to a pre-formed azide or alkyne-terminated SAM.[33] Our strategy provides great flexibility over the peptide or peptide combination presented at each spot without the need to generate entire peptide-conjugated alkanethiol molecules. By forming peptide-conjugates in solution, we avoid complications involving steric effects of bulky molecules assembling on the surface. In this way, any small molecule or ligand containing an alkyne group can be tethered to the microarray surface.

Cell adhesion and spreading on peptide microarrays

To optimize our spot size and reproducibility, we experimented with a number of buffer solutions and incubation conditions for the generation of well-defined arrays. We initially found that the mixed buffer containing H_2O, ethanol, and DMSO evaporated rapidly within 1 minute after spotting, giving poor spot fidelity after cell seeding. We judged spot fidelity by how well the cells adhered and remain localized in circular spots of peptides known to mediate adhesion (YIGSR). To improve spot fidelity, we investigated various buffer additives, incubation and cleaning methods. We experimented with a number of additives and found that a small amount of glycerol (3–10%) greatly improved spot fidelity. Substrate and incubation time also had large effects on the microarray spots. Long incubation times post-spotting generally lead to non-specific adhesion and spots with low definition, possibly due to spreading of the alkanethiol spots. We observed optimal results with low concentrations of glycerol (3–10%) with spotted surfaces washed immediately (Fig. 5). Our trials with various spotting techniques indicate the importance of substrate cleanliness in the formation of well-defined spot sizes. Minimal exposure to atmospheric conditions as well as minimal disruption to the deposited gold improved spot size and homogeneity. However, long post-spotting incubation times even in dessicator and low vacuum conditions appeared to favor breakdown of well-defined microarray spots.

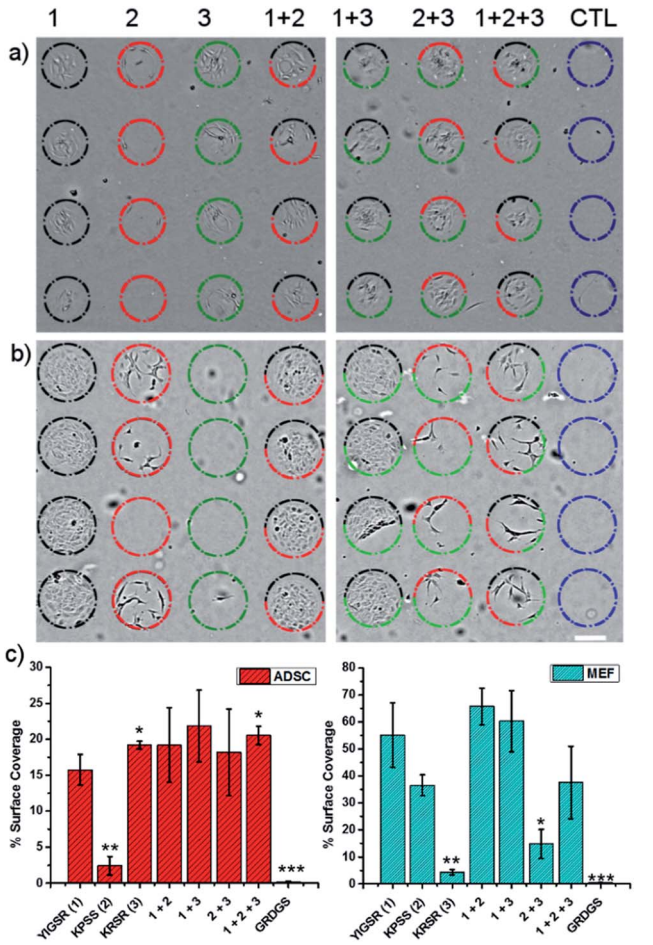

Fig. 5 Brightfield images and quantification of % surface coverage of ADSC (a) and MEF (b) on various peptide spots. Scale bar = 200 μm. *p-value < 0.05, **p-value < 0.01, ***p-value < 0.001 by one-way ANOVA.

This may be related to non-specific spreading of alkanethiols to the intervening background regions.

The synthesis of novel biomimetic materials requires an understanding of the complex components of the extracellular matrix (ECM) and their interactions with one another. In a recent review, Hudalla and Murphy highlight strategies wherein growth factors and glycosaminoglycans can be incorporated into biomaterials to regulate stem cell behavior.[34] We used our peptide microarrays to screen cell adhesion characteristics on combinations of an adhesion peptide YIGSR,[35] a growth factor peptide derived from bone morphogenetic protein 7 (BMP-7),[36] and a heparan sulfate binding peptide (KRSR) known to promote attachment of osteoblasts.[37] We spotted each of these peptides individually as well as in combination and examined the adhesion characteristics of human adipose derived stem cells (ADSCs) as well as mouse embryonic fibroblasts (MEFs) after 3 days in culture. Cells displayed differential adhesion characteristics depending on the peptide ligands they were seeded on and remained confined in spots for over 10 days in culture (Fig. S3†). We quantified "% surface coverage" within each spot, where surface coverage is defined by the fraction of the spot occupied by a given cell type (Fig. S4†). For ADSCs we see similar levels of surface coverage on YIGSR and KRSR surfaces, as well as on all combinations (Fig. 5a and c). Interestingly, KPSS surfaces, which have been shown to enhance osteoblast spreading,[36] had low levels of adhesion of ADSCs, while KRSR, also shown to promote osteoblast attachment,[37] had high levels of ADSC coverage. Even though both peptides may promote adhesion of osteoblasts, the difference in spreading of ADSCs may suggest that they bind to osteoblasts *via* different mechanisms. For MEFs we observed relatively high coverage on KPSS peptides, and very low adherence to KRSR peptide (Fig. 5b). The combination of YIGSR and KPSS displayed the highest surface coverage, while a combination of KPSS and KRSR displayed significantly lower coverage (~50% of coverage on KPSS). The combination of all three peptides had coverage similar to just KPSS. We reason that these differences in surface coverage are due to approximately one-half and one-third of the surface occupied by the KRSR peptide respectively, which does not support fibroblast adhesion.[37] This is in contrast to ADSCs, in which KRSR peptide and combinations containing this peptide show high surface coverage. Also unlike ADSCs, MEFs seem to much more readily adhere to surfaces presenting the BMP7 peptide. Importantly, we spotted a scrambled peptide GRDGS that showed no cell adhesion for either cell types (Fig. 5), indicating that adhesion characteristics are based on the defined peptide ligand rather than non-specific protein adsorption. These results demonstrate that this microarray platform can be a useful tool to screen the adhesion properties of various cell types to different peptide ligands. The contrasting spreading properties of ADSCs and MEFs on KPSS and KRSR peptides suggest that these peptides bind to different cellular receptors that are differentially regulated between these cell types.

ADSC differentiation on combinatorial peptide surfaces

BMP-7 has been successfully tested in animal models and clinical trials for bone fusion and regeneration.[38,39] We hypothesized that a surface presenting a BMP-7 derived peptide may preferentially promote multipotent ADSCs to differentiate into bone. Since we determined based on our microarray assay that KPSS only weakly supports ADSC adhesion, we chose to examine cell adhesion peptides GRGDS[12] and YIGSR, and their combination with BMP-7 peptide KPSS. To assess differences in differentiation for ADSCs cultured on these various peptide combinations for extended times, we cultured cells on ~1 cm^2 peptide conjugated surfaces for 21 days in basal and osteogenic media. Cells were subsequently fixed and stained for runt-related transcription factor 2 (Runx2) (Fig. 6a), a master transcription factor associated with osteogenic differentiation, and osteopontin (OPN) (Fig. 6b), a later stage osteogenic marker. We observed low levels of adhesion on KPSS peptide surfaces, in agreement with our microarray screen. However in basal media conditions, adherent cells on these surfaces had significantly higher intensity of Runx2 (Fig. 6c) and OPN (Fig. 6d) compared to the adhesion peptides GRGDS and YIGSR. Combinations of GRGDS with KPSS and YIGSR with KPSS also had significantly

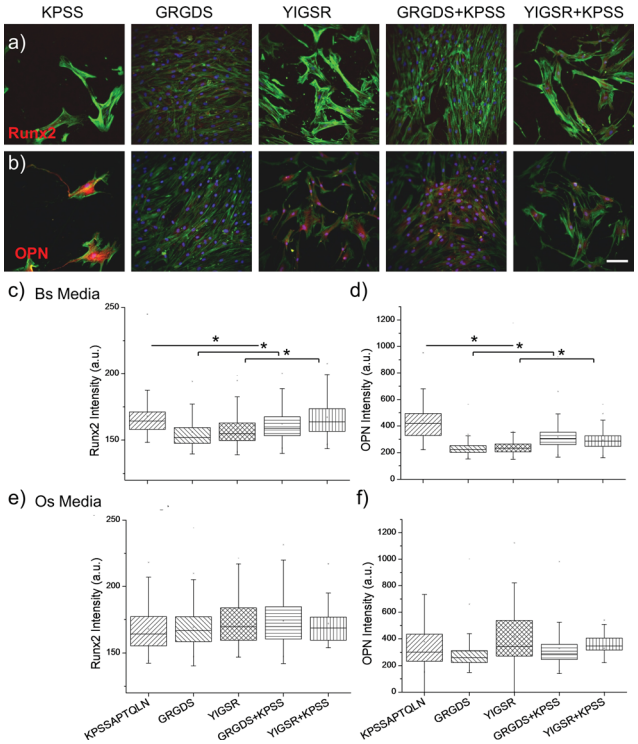

Fig. 6 Immunofluorescence images of ADSCs cultured 3 weeks on peptide combinations. Green = actin, blue = nuclei, red = Runx2 (a) or OPN (b). Scale bar = 200 μm. In basal media, quantification of Runx2 mean intensity (c) and OPN mean intensity (d) between the peptide surfaces. (*) denotes significant difference between groups ($p < 0.05$). In osteogenic media, the differences in Runx2 (e) and OPN (f) expression between the surfaces were not significant.

higher expression of Runx2 and OPN than the adhesion peptide alone. In osteogenic media, we observed no significant differences in either Runx2 (Fig. 6e) or OPN (Fig. 6f) on these various peptide surfaces. Classically, osteogenic differentiation *in vitro* is performed using supplemented media containing a milieu of pro-osteogenic factors, especially dexamethasone, beta-glycerophosphate, ascorbic acid, and other growth factors.[40] We hypothesize that the effects of these factors in the osteogenic media condition abrogated any differences that the peptide surfaces may have had on cultured cells.

BMP-7 has been shown to upregulate Runx2 and promote an osteogenic phenotype in precursor cells.[41,42] A study by Knippenberg *et al.* using BMP-2 and BMP-7 and adipose derived stem cells found BMP-7 actually downregulated osteogenesis and stimulated a chondrogenic phenotype.[43] However, the role of BMP-7 in promoting both chondrogenesis and osteogenesis is documented and is dependent upon cell, media, and culture conditions.[44] Using biomimetic peptides rather than entire bone morphogenetic proteins may provide a more controlled condition to investigate ligand effects on cell fate since proteins may have multiple competing interaction sites as well as tertiary structures. We observed elevated levels of Runx2 and OPN expression on BMP-7 derived KPSS peptide alone and in combination with fibronectin and laminin derived adhesion peptides GRGDS and YIGSR (Fig. 6c and d). This result is similar to that of Zouani *et al.*, who grafted RGD peptides on poly(ethylene terephthalate) with biomimetic peptides derived from the knuckle epitope of BMP-2,7, and 9 and saw upregulation of Runx2 and production of extracellular matrix.[45] He and colleagues reported similar results using a BMP-2 derived peptide in conjunction with RGD on a hydrogel substrate.[46] Biomaterials and drug delivery systems incorporating BMPs appear to be a promising way to improve bone formation while reducing costs of large-scale production of recombinant BMPs.[47,48] Limitations to these materials involve determining optimal density of peptides, as well as preventing non-specific adsorption of proteins.[47] Our self-assembled monolayer based microarray platform allows us to address both these issues. This approach allows us to investigate the specific effects of ligand combinations, while giving us flexibility to easily tune ligand density ratios and compositions. For instance, Kilian and Mrksich investigated the effect of ligand density on mesenchymal stromal cells. They reported that high affinity ligand promoted osteogenic fate decisions, while low affinity ligands could promote either muscle or neural differentiation based on ligand density.[49] Rezania and Healy also examined the importance of ligand density by demonstrating that adhesion and differentiation on mixed peptide surfaces are dependent on cell type as well as the ratio of peptide ligands. They investigated an RGD peptide with a heparin-binding peptide FHRRIKA in 25 : 75, 50 : 50, and 75 : 25 ratios and found a 50 : 50 or 75 : 25 ratio of RGD to FHRRIKA promoted greater spreading and mineralization for RCO cells.[50] The importance of peptide ligand density when presented in combination has been further illuminated by Murphy and colleagues who demonstrated that growth factor binding peptides can be agonists or antagonists depending on the density of presentation.[51] With the platform presented here, researchers may tune ligand affinity and density, as well as investigating effects of combinations of ligands in different ratios.

Conclusions

Our results demonstrate a simple procedure to form peptide microarrays in a single-step using the robust azide–alkyne cycloaddition reaction. Cells seeded onto the spotted regions remain localized for over a week, allowing for the use of this method for long-term culture experiments. We demonstrated the utility of this platform for cell biology investigations by exploring a combination of an adhesion peptide and BMP-7 derived peptide combination and found that the presence of the BMP-7 peptide promoted the expression of osteogenic markers Runx2 and OPN. We anticipate this technique will be useful in the future for screening many different growth factor and adhesion peptides, at variable densities and in combination, for a variety of cell types.

Acknowledgements

This work was supported by the American Cancer Society, Illinois Division Grant #281225. We gratefully acknowledge Michael Sun for assistance in generating SAM surfaces, and Dr Jianjun Cheng for assistance with FTIR. XPS, Ellipsometry, and

AFM was carried out in the Frederick Seitz Materials Research Laboratory Central Facilities, University of Illinois. We thank Dr Rick Haasch in the center for Microanalysis of Materials at the Frederick Seitz Materials Research lab at UIUC for assistance with XPS measurements, Amr Abdeen for assistance with AFM measurements, and Neil Kruger for assistance with ellipsometry measurements. The Bruker UltrafleXtreme MALDI TOFTOF mass spectrometer was purchased in part with a grant from the National Center for Research Resources, National Institutes of Health (S10 RR027109 A).

Notes and references

1 A. J. Friedenstein, R. K. Chailakhlan, K. S. Lalykina and R. K. Chailakhjan, *Cell Tissue Kinet.*, 1970, **3**, 393–403.
2 M. F. Pittenger, A. M. Mackay, S. C. Beck, R. K. Jaiswal, R. Douglas, J. D. Mosca, M. A. Moorman, D. W. Simonetti, S. Craig and D. R. Marshak, *Science*, 1999, **284**, 143–147.
3 F. P. Barry and J. M. Murphy, *Int. J. Biochem. Cell Biol.*, 2004, **36**, 568–584.
4 A. I. Caplan, *J. Pathol.*, 2009, **217**, 318–324.
5 L. da Silva Meirelles, P. C. Chagastelles and N. B. Nardi, *J. Cell Sci.*, 2006, **119**, 2204–2213.
6 A. Schäffler and C. Büchler, *Stem Cells*, 2007, **25**, 818–827.
7 H. Mizuno, M. Tobita and A. C. Uysal, *Stem Cells*, 2012, **30**, 804–810.
8 P. A. Zuk, M. Zhu, H. Mizuno, J. Huang, J. W. Futrell, A. J. Katz, P. Benhaim, H. P. Lorenz and M. H. Hedrick, *Tissue Eng.*, 2001, **7**, 211–228.
9 H. Shin, S. Jo and A. G. Mikos, *Biomaterials*, 2003, **24**, 4353–4364.
10 D. G. Anderson, S. Levenberg and R. Langer, *Nat. Biotechnol.*, 2004, **22**, 863–866.
11 C. J. Flaim, S. Chien and S. N. Bhatia, *Nat. Methods*, 2005, **2**, 119–125.
12 M. D. Pierschbacher and E. Ruoslahti, *Nature*, 1984, **309**, 30–33.
13 E. Ruoslahti, *Annu. Rev. Cell Dev. Biol.*, 1996, **12**, 697–715.
14 G. A. Hudalla and W. L. Murphy, *Langmuir*, 2009, **25**, 5737–5746.
15 S. P. Massia and J. A. Hubbell, *J. Cell Biol.*, 1991, **114**, 1089–1100.
16 J. C. Love, L. A. Estroff, J. K. Kriebel, R. G. Nuzzo and G. M. Whitesides, *Chem. Rev.*, 2005, **105**, 1103–1169.
17 B. T. Houseman and M. Mrksich, *Biomaterials*, 2001, **22**, 943–955.
18 G. A. Hudalla and W. L. Murphy, *Langmuir*, 2010, **26**, 6449–6456.
19 M. P. Lutolf, P. M. Gilbert and H. M. Blau, *Nature*, 2009, **462**, 433–441.
20 S. Gobaa, S. Hoehnel, M. Roccio, A. Negro, S. Kobel and M. P. Lutolf, *Nat. Methods*, 2011, **8**, 949–955.
21 B. P. Orner, R. Derda, R. L. Lewis, J. A. Thomson and L. L. Kiessling, *J. Am. Chem. Soc.*, 2004, **126**, 10808–10809.
22 R. J. Giordano, M. Cardó-Vila, J. Lahdenranta, R. Pasqualini and W. Arap, *Nat. Med.*, 2001, **7**, 1249–1253.
23 R. Derda, S. Musah, B. P. Orner, J. R. Klim, L. Li and L. L. Kiessling, *J. Am. Chem. Soc.*, 2010, **132**, 1289–1295.
24 W. Luo, E. W. L. Chan and M. N. Yousaf, *J. Am. Chem. Soc.*, 2010, **132**, 2614–2621.
25 C. Pale-Grosdemange, E. S. Simon, K. L. Prime and G. M. Whitesides, *J. Am. Chem. Soc.*, 1991, **113**, 12–20.
26 S. Ciampi, T. Böcking, K. A. Kilian, M. James, J. B. Harper and J. J. Gooding, *Langmuir*, 2007, **23**, 9320–9329.
27 M. Mrksich, *ACS Nano*, 2008, **2**, 7–18.
28 J. Su and M. Mrksich, *Langmuir*, 2003, **19**, 4867–4870.
29 B. Zhu, T. Eurell, R. Gunawan and D. Leckband, *J. Biomed. Mater. Res.*, 2001, **56**, 406–416.
30 S. J. Stranick, A. N. Parikh, Y.-T. Tao, D. L. Allara and P. S. Weiss, *J. Phys. Chem.*, 1994, **98**, 7636–7646.
31 R. K. Smith, P. A. Lewis and P. S. Weiss, *Prog. Surf. Sci.*, 2004, **75**, 1–68.
32 R. Chelmowski, S. D. Köster, A. Kerstan, A. Prekelt, C. Grunwald, T. Winkler, N. Metzler-Nolte, A. Terfort and C. Wöll, *J. Am. Chem. Soc.*, 2008, **130**, 14952–14953.
33 R. Chelmowski, D. Käfer, S. D. Köster, T. Klasen, T. Winkler, A. Terfort, N. Metzler-Nolte and C. Wöll, *Langmuir*, 2009, **25**, 11480–11485.
34 G. A. Hudalla and W. L. Murphy, *Adv. Funct. Mater.*, 2011, **21**, 1754–1768.
35 J. Graf, R. C. Ogle, F. A. Robey, M. Sasaki, G. R. Martin, Y. Yamada and H. K. Kleinman, *Biochemistry*, 1987, **26**, 6896–6900.
36 Y. Chen and T. J. Webster, *J. Biomed. Mater. Res., Part A*, 2009, **91**, 296–304.
37 K. C. Dee, T. T. Andersen and R. Bizios, *J. Biomed. Mater. Res.*, 1998, **40**, 371–377.
38 A. P. White, A. R. Vaccaro, J. A. Hall, P. G. Whang, B. C. Friel and M. D. McKee, *Int. Orthop.*, 2007, **31**, 735–741.
39 P. Simic and S. Vukicevic, *EMBO Rep.*, 2007, **8**, 327–331.
40 C. Vater, P. Kasten and M. Stiehler, *Acta Biomater.*, 2011, **7**, 463–477.
41 P. Ducy, R. Zhang, V. Geoffroy, A. L. Ridall and G. Karsenty, *Cell*, 1997, **89**, 747–754.
42 K. Gu, L. Zhang, T. Jin and R. B. Rutherford, *Cells Tissues Organs*, 2004, **176**, 28–40.
43 M. Knippenberg, M. N. Helder, B. Zandieh Doulabi, P. I. J. M. Wuisman and J. Klein-Nulend, *Biochem. Biophys. Res. Commun.*, 2006, **342**, 902–908.
44 B. Shen, A. Wei, S. Whittaker, L. A. Williams, H. Tao, D. D. F. Ma and A. D. Diwan, *J. Cell. Biochem.*, 2010, **109**, 406–416.
45 O. F. Zouani, C. Chollet, B. Guillotin and M.-C. Durrieu, *Biomaterials*, 2010, **31**, 8245–8253.
46 X. He, J. Ma and E. Jabbari, *Langmuir*, 2008, **24**, 12508–12516.
47 H. Senta, H. Park, E. Bergeron, O. Drevelle, D. Fong, E. Leblanc, F. Cabana, S. Roux, G. Grenier and N. Faucheux, *Cytokine Growth Factor Rev.*, 2009, **20**, 213–222.
48 H. Senta, E. Bergeron, O. Drevelle, H. Park and N. Faucheux, *Can. J. Chem. Eng.*, 2011, **89**, 227–239.
49 K. A. Kilian and M. Mrksich, *Angew. Chem., Int. Ed.*, 2012, **51**, 4891–4895.
50 A. Rezania and K. E. Healy, *Biotechnol. Prog.*, 1999, **15**, 19–32.
51 J. T. Koepsel, E. H. Nguyen and W. L. Murphy, *Integr. Biol.*, 2012, **4**, 914–924.

